

Original Article

Model-Based Diagnosis of an Eccentricity Fault in a Dynamic Gear System

Yakeu Happi Kemajou Herbert¹, Tchomeni Kouejou Bernard Xavier², Alfayo Anyika Alugongo³

^{1,2,3}Vaal University of Technology, Department of Industrial Engineering, Operation Management and Mechanical Engineering, South Africa.

¹Corresponding Author : kemajouy@vut.ac.za

Received: 18 December 2024

Revised: 03 April 2025

Accepted: 10 June 2025

Published: 28 June 2025

Abstract - This paper employs a nine-degree-of-freedom dynamic model, considering torsional and lateral motions, to analyse the dynamic characteristics of a two-stage spur gear system. The model incorporates gear eccentricity faults and dynamic transmission errors by establishing a mesh stiffness model. The differential vibration equations for the spur gear system are derived using the Lagrangian method. Numerical simulations are conducted using a combination of the Short-Term Fourier Transform (STFT), 3D Waterfall FFT (Fast Fourier Transform), and RPM-frequency mapping technique under various operating scenarios. Analysing the responses imposed by the system under both regular and chaotic vibrations reveals that gear eccentricity faults significantly impact the system's performance. The frequency content changes over time and 3D plots provide a more detailed frequency-RPM representation, allowing the detection of transient faults in gears compared to the time domain and frequency domain. Theoretical analysis confirms the effectiveness of the STFT and 3D Waterfall FFT-based frequency-RPM transmission error detection approach.

Keywords - Eccentricity fault, Gear mesh stiffness, RPM-Frequency map – STFT, 3D Waterfall FFT, Transmission error, Two-stage spur gear system.

1. Introduction

In industry, mechanical gearboxes drive rotating machinery such as robots, aircraft engines, manufacturing equipment, and wind turbines. Vibrations generated by its operation change the machine's behaviour and speed up the wear of specific mechanical components such as gear teeth, bearings and others. These signals may change due to a vibrating structure modification at the defect formation time [1]. For this, many studies focus on torsional vibration analysis or lateral torsion by developing numerical models of gear dynamics. A high-precision gear transmission system can be challenging to produce and assemble. One common issue in gear systems is gear eccentricity, caused by manufacturing and making errors. In wind power, eccentricity can cause transmission errors of up to 10%, reducing the transmission ratio. In high-precision robotic systems, a slight deviation can lead to high energy consumption and positioning errors. This can lead to complex modulations and dynamic excitations, ultimately degrading the gear system's dynamic performance [2]. The primary cause of significant variations in Transmission Error (TE) and fluctuating backlash in gear transmission is eccentricity error. Manufacturing and assembly processes can introduce eccentricity errors, leading to periodic fluctuations in TE and backlash. This degradation in transmission precision and

backlash adjustment accuracy underscores the importance of studying gear eccentricity errors. Understanding and addressing these errors are crucial for improving transmission precision and maximizing backlash compensation or correction. The effects of mounting defects, such as misalignment eccentricity and shape abnormalities, on gear dynamics were examined by Vexex and Maatar [3], who developed a new lumped parameter model to clarify the drawbacks of eccentricity. Wang et al. [4] used a dynamic Finite Element Model (FEM) to study the interaction between tooth eccentricity, backlash and transmission error in two-stage gear systems. Researchers have identified and developed methods to detect and diagnose faults by examining the vibration signals produced during meshing. Parey and Tandon [5] and Rigaud [6] have developed a dynamic modelling approach based on discretization using finite elements for all elastic transmission components, including gears, shafts, bearings, and casing. Saxena, Parey, and Chouksey [7] considered sliding friction in their study to provide an analytical approach for determining the Time-Varying Meshing Stiffness (TVMS) of spur gears for different spall forms, sizes, and positions. Building on previous research on the dynamic analysis of gear transmission systems affected by gear eccentricities, a dynamic model for a cylindrical gear rotor system was developed by Yu et al. [8],



considering a local tooth profile error as well as a global assembly error. This model integrates a Finite Element (FE)-based model for the shaft structure, a lumped parameter bearing model, and a 3D gear model. Aijun et al. [9] investigated a multi-stage planetary transmission system's mathematical model to study gears' dynamic response affected by profile defects and assembly errors, which subsequently caused crack-like failures.

Time-series imaging and FFT spectrum methods were used to analyze the dynamic response. Yifan et al. and Wang et al. references [10-11] proposed a time-frequency imaging method that includes several oscillatory components with time-varying amplitude and frequency to diagnose gear faults under varying speeds. Although many studies have been conducted on gear dynamics, only a few studies have comprehensively investigated the influence of eccentricity on coupling stiffness and nonlinear oscillatory responses using time-frequency methods such as STFT and RPM frequency methods. Time-frequency analysis to simultaneously decompose signals in both time and frequency and prioritise between resolutions to capture transient responses.

Therefore, it is crucial to establish appropriate analyses and methodologies for problem detection to investigate the mechanisms of fault diagnosis. The primary objective of this study is to examine the effects of gear eccentricity on the meshing stiffness and dynamic behaviour of a two-stage spur gear system. A dynamic model was implemented to achieve this goal, considering stiffness and error excitations. The research focuses on the effect of eccentricity factors on the variable stiffness of the network and their impact on the

dynamic properties of the system, especially when studying anomalies in weathering and spur gears. This study uniquely uses a nine-degree-of-freedom dynamic model, including eccentricity error and time-frequency analysis (combines STFT, 3D Waterfall FFT and RPM map) to identify anomalies accurately. The STFT, 3D waterfall FFT and frequency-RPM mapping methods are implemented to facilitate the detection and diagnosis of eccentricity irregularities. The state eccentricity of the system under study allows the development of analytical methods dedicated explicitly to this configuration.

The influence of gear eccentricity on the lateral, torsional, and TE dynamic responses is studied in various scenarios. In this paper, Section 2 provides a comprehensive description of the selected two-stage spur gear. In Section 3, the analysis considers the detection of gear eccentricity by examining its effects on the mesh stiffness. Section 4 presents the governing equation for the mathematical dynamic modelling of a double-stage spur gear system. Section 5 analyses the eccentricity impact on the two-stage gear system vibration characteristics at 0 mm, 50 mm, and 100 mm. Section 6 draws a comparative discussion between the time-frequency analysis techniques and traditional analysis used in previous research. Finally, conclusions are drawn in Section 7.

2. Spur Gear System Model

Figure 1 shows a two-stage oscillating gear modelled without initial impact or friction. The gear transmission mechanisms are modelled as rigid rollers with friction stiffness that simulate the gears' elastic behaviour, assuming full contact efficiency between the pinion and gear.

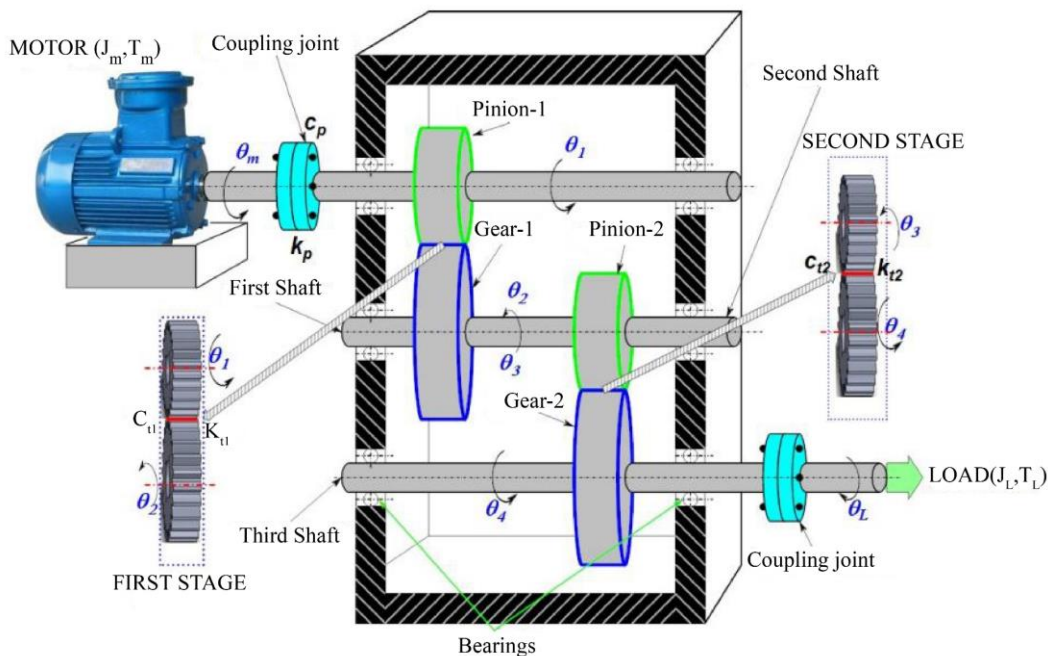


Fig. 1 Dynamic model of a gear system with two stages

3. Meshing Stiffness Model of a Spur Gear

The method for calculating mesh stiffness is derived from the potential energy approach initially proposed by Yang and Lin [12] and subsequently enhanced by Tian [13] and Sainsot et al. [14].

The evaluation of the gear system is carried out through the use of mesh stiffness, which is associated with two developing gear profiles with faultless accuracy, as illustrated in Figure 2. Two gears in the mesh are visible in Figure 2, where $2 \times bt$ is indicated. In this Figure, bt stands for the tooth face width of one gear tooth. In the mesh, the gears are depicted as a pair that transfers torque and motion from one to the other.

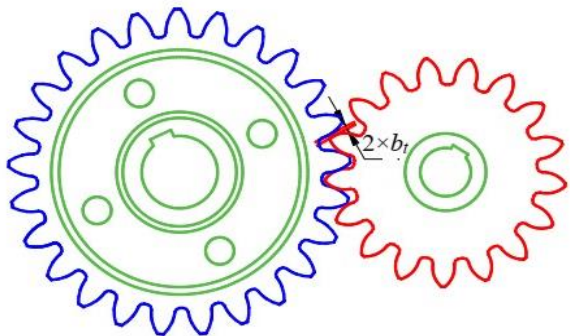


Fig. 2 Two involute gear profiles

In Figure 3, the involute of a circle is defined as the curve traced by a point N on a defect-free base circle as it rolls along a straight line. The curve is generated as point N moves away from the circle while keeping a taut, rigid line under constant tension. The length of the unwound line at any moment equals the distance from point N to the base circle.

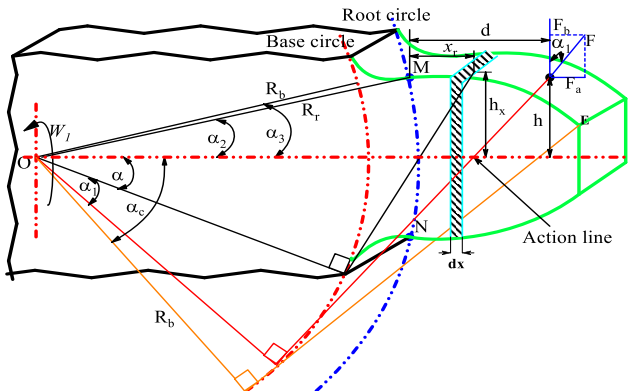


Fig. 3 The root circle of a spur gear tooth beam model exceeds the size of the base circle

Using the beam theory, Hertzian, bending, shear, and axial compression energies in a gear tooth can be illustrated as follows:

$$\begin{cases} U_h = \frac{1}{2} \frac{F^2}{k_{Hertz}} = \frac{4(1-\nu^2)}{\pi EL} \\ U_b = \frac{1}{2} \frac{F^2}{k_b} = \int_0^d \frac{(F_b(d-x) - M)^2}{2EI_x} dx & 0 < x < d \\ U_a = \frac{1}{2} \frac{F^2}{k_a} = \int_0^d \frac{F_a^2}{2EA_x} dx & 0 < x < d \\ U_s = \frac{1}{2} \frac{F^2}{k_s} = \int_0^d \frac{1.2F_b^2}{2GA_x} dx & 0 < x < d \end{cases} \quad (1)$$

Bending, shear and axial compression stiffness in the direction of the force F is denoted by k_b , k_s and k_a , and respectively. As demonstrated in Figure 3, the action force F can be decomposed into two perpendicular forces: the axial force F_b and the bending force F_a . They are stated as follows:

$$\begin{cases} F_a = F \sin \alpha_1 \\ F_b = F \cos \alpha_1 \end{cases} \quad (2)$$

Equation (3) uses the following expression to get the tooth x 's profile, which is described by its involute geometry (becomes the integration variable instead of x).

$$x = R_b \cos \alpha - R_b (\alpha_2 - \alpha) \sin \alpha - R_b \cos \alpha_2 - R_r \cos \alpha_3 \quad (3)$$

Its derivative is obtained as follows:

$$dx = R_b (\alpha - \alpha_2) \cos \alpha d\alpha \quad (4)$$

The shear modulus G , moment of inertia of the tooth's surface I_x , couple M , and section area A_x are expressed as given in Equation (5) and subsequently replaced into U_h , U_b , U_a , and U_s formulas, respectively, based on the geometry of the involute tooth in Figure. 3.

$$\begin{cases} M = F_a \times h, \text{ thus, } h = R_b [(\alpha_1 + \alpha_2) \cos \alpha_1 \cdot \sin \alpha_1] \\ G = \frac{E}{2(1+\nu)} \\ A_x = 2 \times h_x \times L \\ I_x = \frac{1}{12} (2h_x)^3 L, \text{ thus, } h_x = R_b [(\alpha_2 - \alpha) \cos \alpha + \sin \alpha] \\ d = R_b [(\alpha_1 + \alpha_2) \sin \alpha_1 + \cos \alpha_1] - R_r \cos \alpha_3 \end{cases} \quad (5)$$

L represents the tooth width, E denotes Young's modulus and Poisson's ratio. α_2 represents the half-tooth angle on the fundamental circle, α_3 illustrates the approximate half-tooth angle on the root circle and symbolizes the angular movement.

Following the replacement of all the expressions of equation (5) by those of equation (1) and taking into account that the root circle (R_r) is greater than the base circle (R_b), also known as the dedendum circle, it can be expressed the equations relating to the stiffness according to Hertz, the bending, axial and shear of the tooth in its optimal state as shown in Figure 2:

$$\left\{ \begin{aligned} k_{hertz} &= \frac{\pi EL}{4(1-\nu^2)} \\ \frac{1}{k_b} &= \int_{-\alpha_1}^{\alpha_2} \frac{3[1 + \cos\alpha_1(-\cos\alpha + (\alpha_2 + \alpha)\sin\alpha)]^2 (\alpha - \alpha_2) \cos\alpha \, d\alpha}{2EL((\alpha_2 - \alpha)\cos\alpha + \sin\alpha)^3} \\ \frac{1}{k_a} &= \int_{-\alpha_1}^{\alpha_2} \frac{\sin\alpha_1^2 R_b (\alpha_2 - \alpha) \cos\alpha}{2EL[(\alpha_2 - \alpha)\cos\alpha + \sin\alpha]} d\alpha \\ \frac{1}{k_s} &= \int_{-\alpha_1}^{\alpha_2} \frac{1.2(1+\nu)\cos\alpha_1^2 (\alpha_2 - \alpha) \cos\alpha}{EL[(\alpha_2 - \alpha)\cos\alpha + \sin\alpha]} d\alpha \end{aligned} \right. \quad (6)$$

The total potential energy U stored in the meshing gear system includes the Hertz energy U_h , the bending energy U_b , the axial compression energy U_a and the shear energy U_s . It can be expressed using the following equation:

$$U_t = \frac{F^2}{2k_m} = U_h + U_b + U_s + U_a = \frac{F^2}{2} \left(\frac{1}{k_h} + \frac{1}{k_b} + \frac{1}{k_s} + \frac{1}{k_a} \right) \quad (7)$$

Considering the first phase of the pinion gear mechanism, influenced by the eccentricity error, the stiffnesses corresponding to the Hertz effect, bending, shear and axial compression vary accordingly to k_h , k_{b1} , k_{s1} , and k_{a1} in

sequences. Thus, the expression for the total effective mesh stiffness for a double-stage spur gear is:

$$k_{total} = k_{t_1}(\text{First stage}) + k_{t_2}(\text{Second stage}) \quad (8)$$

$$k_{t_1}(\text{First stage}) = \frac{\overbrace{1}^{\text{affected by eccentricity}}}{\underbrace{\frac{1}{k_h} + \frac{1}{k_{b_1}} + \frac{1}{k_{s_1}} + \frac{1}{k_{a_1}}}_{\text{driving gear(pinion)}} + \underbrace{\frac{1}{k_{b_2}} + \frac{1}{k_{s_2}} + \frac{1}{k_{a_2}}}_{\text{driven gear(wheel)}}}$$

$$k_{t_2}(\text{Second stage}) = \frac{1}{\underbrace{\frac{1}{k_h} + \frac{1}{k_{b_3}} + \frac{1}{k_{s_3}} + \frac{1}{k_{a_3}}}_{\text{health driving gear(pinion)}} + \underbrace{\frac{1}{k_{b_4}} + \frac{1}{k_{s_4}} + \frac{1}{k_{a_4}}}_{\text{health driven gear(wheel)}}} \quad (9)$$

4. Fault Two-Stage Gear System with Eccentricity Fault

The torque of an electric motor T_{in} drives the gear unit through coupling 1, whose parameters are related to the torsional stiffness and the damping coefficient. The system loads the movement through an output coupling consisting of the following components: k_g for the torsional stiffness and c_g for the damping coefficient, applying a resistance torque (T_{out}) to the output shaft, i.e. shaft 2. The 09-DOF is used to model the two-stage gear. Studying the dynamics of two-stage gear systems with eccentricity faults is crucial for understanding their behavior and performance under such conditions. Table 1 lists the specifications of the two-stage gear system.

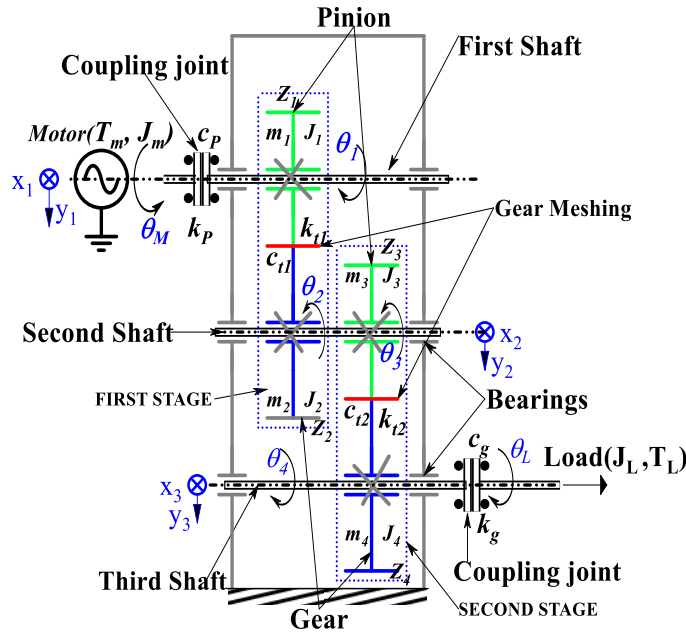


Fig. 4 Schematic representation of a two-stage gear system

Table 1. The two-stage gear under study physical characteristics

Specifications	Stage 1	Stage 2
Young Module (E)	2068×10^{12} Pa	2068×10^{12} Pa
Number of teeth	$Z_1 = 30$ & $Z_2 = 90$	$Z_3 = 30$ & $Z_4 = 90$
Poisson's ratio	3×10^{-1}	3×10^{-1}
Angle of Pressure	20 degrees	20 degrees
Pinion / Gear base circle radius (mm)	$R_1 = 30.1$ & $R_2 = 76.1$	$R_3 = 30.1$ & $R_4 = 76.1$
Mass (kg)	$M_1 = 0.96$ & $M_2 = 2.88$	$M_3 = 0.96$ & $M_4 = 2.88$
Bearings meshing stiffness (Ns/m)	$k_1 = k_3 = 656 \times 10^8$	$k_2 = k_4 = 656 \times 10^8$
Bearings damping coefficient (Ns/m)	$c_1 = c_2 = 18 \times 10^6$	$c_3 = c_4 = 18 \times 10^6$
Coupling torsional stiffness (Ns/m)	$k_p = 44 \times 10^5$	$k_g = 44 \times 10^5$
Coupling damping coefficient (Nms/rad)	$c_p = 5 \times 10^5$	$c_g = 5 \times 10^5$

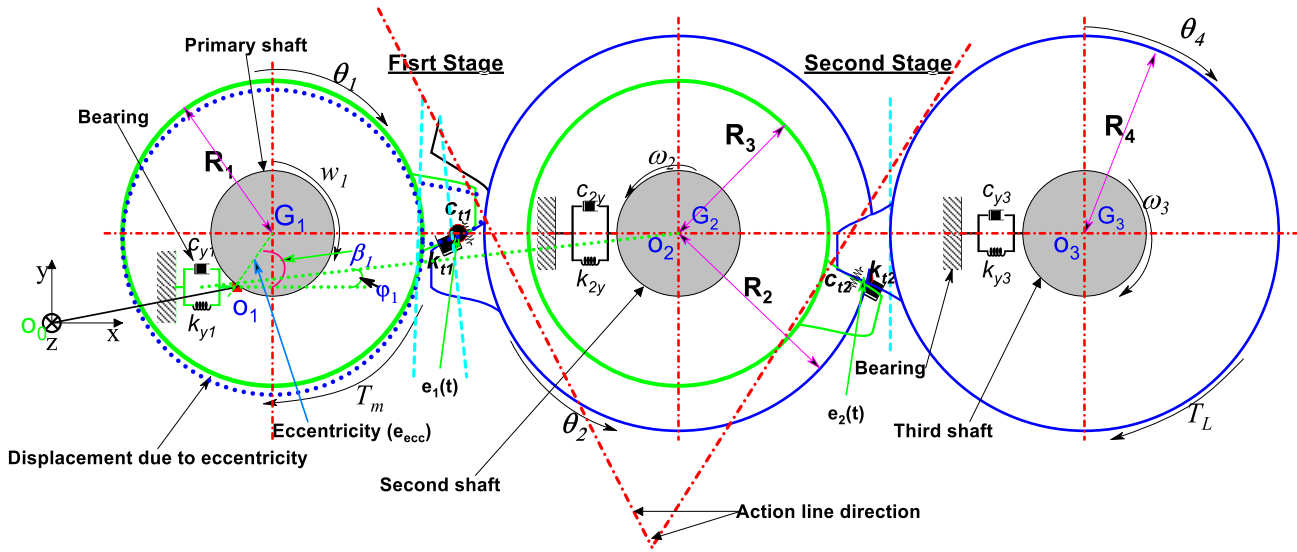


Fig. 5 Gear system with two-stage with eccentricity fault

In Figure 5, since the centre of the pinion pitch circle is not situated on the axis of rotation of the corresponding pinion, this leads to an eccentricity defect that provokes a transmission error. The transmission error $\delta(t)$ is the overall elastic deformation of the teeth at the point of contact of a pair of gears.

4.1. Vibration Differential Equations Derivation

Along the line of action is the actual deformation (relative displacement), denoted as δ . Relative displacement along the pressure line of the gear meshing in stages 1 and 2 can be expressed as follows:

$$\delta_1(t) = (y_1 - y_2) \cos \phi_1 + R_1 \theta_1 - R_2 \theta_2 + e_{ecc} \sin(\beta_1 - \phi_1) + e_1(t), \quad (10)$$

$$\delta_2(t) = (y_2 - y_3) \cos \phi_2 + R_3 \theta_3 - R_4 \theta_4 + e_2(t), \quad (11)$$

$$\phi_1 = \begin{cases} \alpha_1 + (-1)^{n+1} \varphi_1 & \omega_1: \text{Counterclockwise} \\ \alpha_1 + (-1)^n \varphi_1 & \omega_1: \text{Clockwise} \end{cases}, \quad (12)$$

With the subscript n denoting the order of gear mesh (n = 1, 2). Here, it is only considered the most common case $\varphi_1 = 0$. The standard deviation $e_1(t)$ of a pinion eccentricity and total angular displacement of a pinion β_1 is expressed as follows:

$$e_1(t) = e_{amp} \sin(z_1 \omega_1 t + \alpha_1), \quad (13)$$

$$\beta_1 = \omega_1 t + \theta_1, \quad (14)$$

Where e_{amp} is the amplitude of the static transmission error, α_1 is the initial phase angle of the pinion, θ_1 is the pinion's torsional displacement, and ω_1 is the angular velocity of the shaft/pinion. The equation of vibration behavior of a two-stage gearbox can be formulated using dynamic modeling that considers both transverse and torsional vibrations.

According to the Rayleigh energy approach, the study has proven that the transfer of mechanical energy through the gear

teeth is closely associated with two key factors: kinetic energy, associated with the displacements of rotating and linearly moving masses, and potential energy, which mainly arises from the elastic deformations of the teeth when they contact.

The configuration of the gearbox has a significant effect on both types of energy, thereby determining the overall dynamic response of the system.

4.1.1. Kinetic Expression of Energy

By adding the energy of each element of the system, we arrive at the following expression for determining the kinetic energy (T) of the system:

$$T = \frac{1}{2} M_1 \dot{y}_1^2 + \frac{1}{2} M_2 \dot{y}_2^2 + \frac{1}{2} M_3 \dot{y}_3^2 + \frac{1}{2} J_1 \dot{\theta}_1^2 + \frac{1}{2} J_2 \dot{\theta}_2^2 + \frac{1}{2} J_3 \dot{\theta}_3^2 + \frac{1}{2} J_4 \dot{\theta}_4^2 + \frac{1}{2} J_{in} \dot{\theta}_{in}^2 + \frac{1}{2} J_{out} \dot{\theta}_{out}^2 \tag{15}$$

1 and 3 are the designations of the motor gear, while 2 and 4 refer to the driven gear.

4.1.2. Expression of a Potential Function

The total potential energy U of the system is calculated by adding the energy of each element of the system as follows:

$$U = \frac{1}{2} k_{y1} y_1^2 + \frac{1}{2} k_p (\theta_m - \theta_1)^2 + \frac{1}{2} k_{y2} y_2^2 + \frac{1}{2} k_{y3} y_3^2 + \frac{1}{2} k_g (\theta_4 - \theta_l)^2 + \frac{1}{2} k_{t1} [(y_1 + R_1 \theta_1) - (y_2 + R_2 \theta_2)]^2 + \frac{1}{2} k_{t2} [(y_2 + R_2 \theta_2) - (y_3 + R_4 \theta_4)]^2 \tag{16}$$

4.1.3. Expression of Rayleigh Dissipation Function

The Rayleigh dissipation function (D) for a two-speed transfer using various linear viscous dampers is expressed as:

$$D = \frac{1}{2} c_{y1} \dot{y}_1^2 + \frac{1}{2} c_p (\dot{\theta}_m - \dot{\theta}_1)^2 + \frac{1}{2} c_{y2} \dot{y}_2^2 + \frac{1}{2} c_{y3} \dot{y}_3^2 + \frac{1}{2} c_g (\dot{\theta}_4 - \dot{\theta}_l)^2 + \frac{1}{2} c_{t1} [(\dot{y}_1 + R_1 \dot{\theta}_1) - (\dot{y}_2 + R_2 \dot{\theta}_2)]^2 + \frac{1}{2} c_{t2} [(\dot{y}_2 + R_2 \dot{\theta}_2) - (\dot{y}_3 + R_4 \dot{\theta}_4)]^2 \tag{17}$$

4.2. Governing Equations of Gear System

The motions shown in Figure 4 are defined by nine equations, each associated with a degree of freedom.

For the application of Lagrange's formula, the governing equation is:

$$\frac{d}{dt} \left(\frac{\partial T}{\partial \dot{q}} \right) + \frac{\partial D}{\partial \dot{q}} + \frac{\partial U}{\partial q} - \frac{\partial T}{\partial q} = F_q, \quad (q = y_1, y_2, y_3, \theta_1, \theta_2, \theta_3, \theta_4, \theta_m, \theta_{out}) \tag{18}$$

By calculating based on equations (14), (15) and (16), the equations of the gear system motion in matrix form are obtained as follows.

$$\begin{bmatrix} M_1 & 0 & 0 & 0 & 0 & 0 & 0 & 0 & 0 \\ 0 & M_2 & 0 & 0 & 0 & 0 & 0 & 0 & 0 \\ 0 & 0 & M_3 & 0 & 0 & 0 & 0 & 0 & 0 \\ 0 & 0 & 0 & J_1 & 0 & 0 & 0 & 0 & 0 \\ 0 & 0 & 0 & 0 & J_2 & 0 & 0 & 0 & 0 \\ 0 & 0 & 0 & 0 & 0 & J_3 & 0 & 0 & 0 \\ 0 & 0 & 0 & 0 & 0 & 0 & J_4 & 0 & 0 \\ 0 & 0 & 0 & 0 & 0 & 0 & 0 & J_{in} & 0 \\ 0 & 0 & 0 & 0 & 0 & 0 & 0 & 0 & J_{out} \end{bmatrix} \begin{Bmatrix} \ddot{y}_1 \\ \ddot{y}_2 \\ \ddot{y}_3 \\ \ddot{\theta}_1 \\ \ddot{\theta}_2 \\ \ddot{\theta}_3 \\ \ddot{\theta}_4 \\ \ddot{\theta}_{in} \\ \ddot{\theta}_{out} \end{Bmatrix} + \begin{bmatrix} c_{y1} & 0 & 0 & 0 & 0 & 0 & 0 & 0 & 0 \\ 0 & c_{y2} & 0 & 0 & 0 & 0 & 0 & 0 & 0 \\ 0 & 0 & c_{y3} & 0 & 0 & 0 & 0 & 0 & 0 \\ 0 & 0 & 0 & c_{t1} & 0 & 0 & 0 & -c_{t1} & 0 \\ 0 & 0 & 0 & 0 & c_{t2} & -c_{t2} & 0 & 0 & 0 \\ 0 & 0 & 0 & 0 & -c_{t2} & c_{t2} & 0 & 0 & 0 \\ 0 & 0 & 0 & 0 & 0 & 0 & c_{t3} & 0 & -c_{t3} \\ 0 & 0 & 0 & c_{t1} & 0 & 0 & 0 & c_{t1} & 0 \\ 0 & 0 & 0 & 0 & 0 & 0 & -c_{t3} & 0 & c_{t3} \end{bmatrix} \begin{Bmatrix} \dot{y}_1 \\ \dot{y}_2 \\ \dot{y}_3 \\ \dot{\theta}_1 \\ \dot{\theta}_2 \\ \dot{\theta}_3 \\ \dot{\theta}_4 \\ \dot{\theta}_{in} \\ \dot{\theta}_{out} \end{Bmatrix} + \begin{bmatrix} k_{y1} & 0 & 0 & 0 & 0 & 0 & 0 & 0 & 0 \\ 0 & k_{y2} & 0 & 0 & 0 & 0 & 0 & 0 & 0 \\ 0 & 0 & k_{y3} & 0 & 0 & 0 & 0 & 0 & 0 \\ 0 & 0 & 0 & k_{t1} & 0 & 0 & 0 & -k_{t1} & 0 \\ 0 & 0 & 0 & 0 & k_{t2} & -k_{t2} & 0 & 0 & 0 \\ 0 & 0 & 0 & 0 & -k_{t2} & k_{t2} & 0 & 0 & 0 \\ 0 & 0 & 0 & 0 & 0 & 0 & k_{t3} & 0 & -k_{t3} \\ 0 & 0 & 0 & c_{t1} & 0 & 0 & 0 & k_{t1} & 0 \\ 0 & 0 & 0 & 0 & 0 & 0 & -k_{t3} & 0 & k_{t3} \end{bmatrix} \begin{Bmatrix} y_1 \\ y_2 \\ y_3 \\ \theta_1 \\ \theta_2 \\ \theta_3 \\ \theta_4 \\ \theta_{in} \\ \theta_{out} \end{Bmatrix} = \begin{Bmatrix} -F_{t1} \cos \phi_1 + F_c \sin \beta_1 + F_l \cos \beta_1 \\ F_{t1} \cos \phi_1 + F_{t2} \cos \phi_2 \\ -F_{t2} \phi_2 \\ -T_1 + F_l \\ T_2 \\ -T_3 \\ T_4 \\ T_{in} \\ -T_{out} \end{Bmatrix} \tag{19}$$

Where F_{t1} and F_{t2} are the dynamic meshing forces of gear pair 1, affected by the eccentricity fault on the meshing points, is compared to gear pair 2 in perfect condition:

$$\begin{cases} F_{r1} = (\delta_1(t)k_{t_1} + \dot{\delta}_1(t)c_{t_1}) \\ F_{r2} = (\delta_2(t)k_{t_2} + \dot{\delta}_2(t)c_{t_2}) \end{cases} \quad (20)$$

$$\begin{cases} T_1 = R_1(\delta_1(t)k_{t_1} + \dot{\delta}_1(t)c_{t_1}) \\ T_2 = R_2(\delta_1(t)k_{t_1} + \dot{\delta}_1(t)c_{t_1}) \\ T_3 = R_3(\delta_2(t)k_{t_2} + \dot{\delta}_2(t)c_{t_2}) \\ T_4 = R_4(\delta_2(t)k_{t_2} + \dot{\delta}_2(t)c_{t_2}) \end{cases} \quad (21)$$

$T_1, T_2, T_3,$ and T_4 are the torques developed due to the gear meshing forces at stages 1 and 2. F_T and F_C , representing the tangential and centrifugal forces of a gear pair at stage 1 induced by gear eccentricity [28], can be calculated as follows:

$$F_T = M_1 e_1 \ddot{\theta}_1 \quad (22)$$

$$F_C = M_1 e_{ecc} (\dot{\theta}_1 + \omega_1)^2 \quad (23)$$

5. Results

This research combines multi-degree-of-freedom dynamic models with advanced time-frequency analysis techniques to study gear eccentricity, representing a significant innovation.

This study highlights the improvement in transient fault detection compared to traditional FFT methods and provides a new display of how drive shaft stiffness changes with eccentricity, which is still relatively understudied in the current literature.

5.1. Gearbox Vibration Simulation Results

The specified gearbox system is analyzed by considering the assumptions in Table 1. The simulation will use an RPM-frequency map, a 3D FFT waterfall, and an STFT diagnostic technique to accurately identify the features of coupled failures in a spur gear system.

The Runge-Kutta discretization method and a MATLAB solver with the ode45 subroutine are used to solve the equations. At this early stage of the trial, each level of eccentricity has been deemed consequential. Each analysis was simulated for ten seconds.

Figure 6 shows that the system produces a regular, nearly sinusoidal oscillation. A stable amplitude and high frequency indicate a source of regular, cyclical vibrations, characteristic of a steady-state rolling phenomenon and a harmonic imbalance associated with rotation.

This likely indicates stationary behavior when the device operates at a constant speed. However, Figure 7 shows that the

Fourier spectrum indicates that the signal in the time domain is dominated by a single central frequency, proving the observed phenomenon's almost single-frequency nature.

The sharp, pronounced peak at 620 Hz indicates a stable mechanical excitation frequency, which may be related to the gear frequency, rotational unbalance, and structural resonance induced by the system operation.

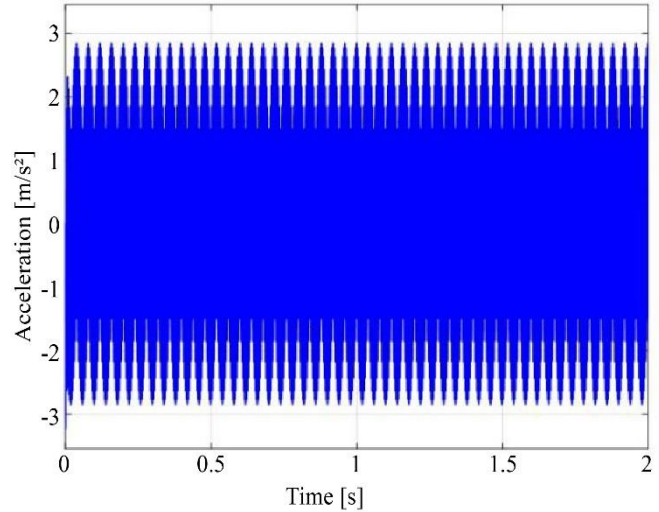


Fig. 6 Healthy gear vibration response

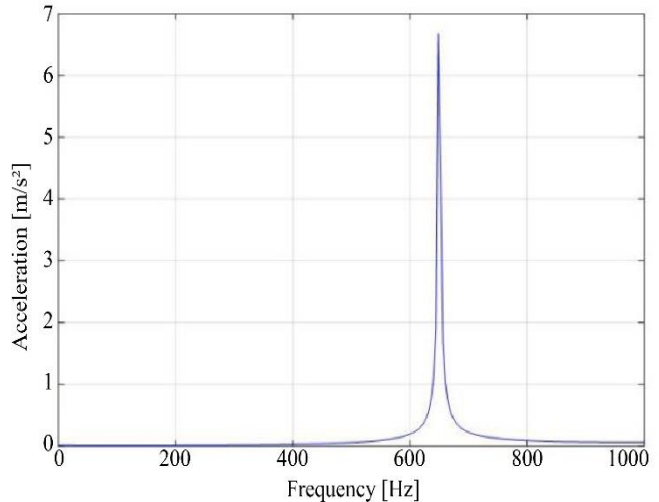


Fig. 7 Spectrum of vibration response of healthy gear

In Figure 8, the signal is periodic but varies in amplitude. It is observed as an amplitude modulation, which indicates the existence of a frequency component that overlaps the frequency.

The deviation is greater than $\pm 4 \text{ m}^2$, a high value for a traditional rotating rotor. This may indicate dynamic failure and possible harmonic excitation, all caused by the eccentricity fault of $50 \text{ }\mu\text{m}$.

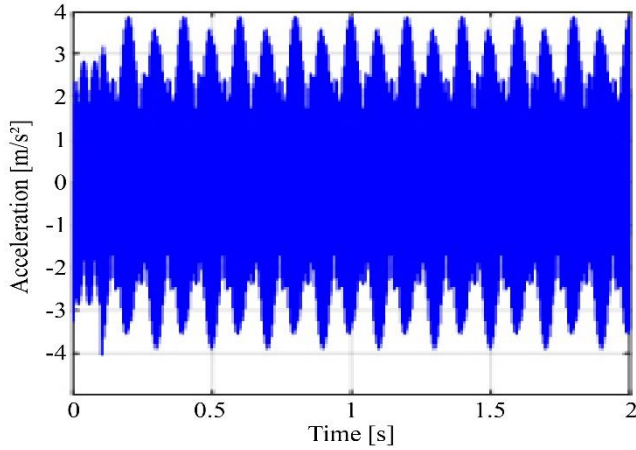


Fig. 8 Gear vibration response with 50 μm eccentricity

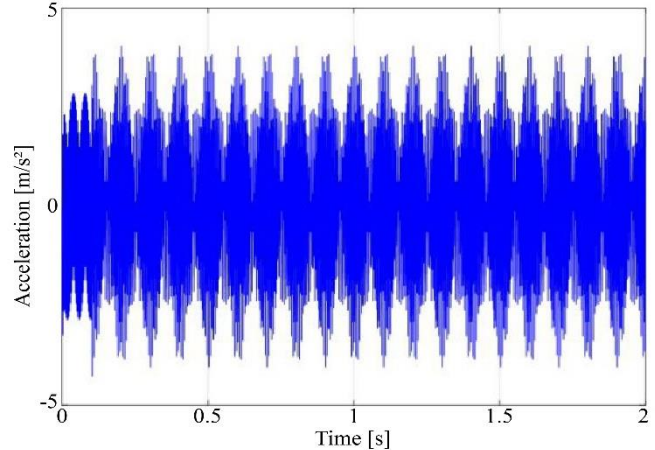


Fig. 10 Gear vibration response with 100 μm eccentricity

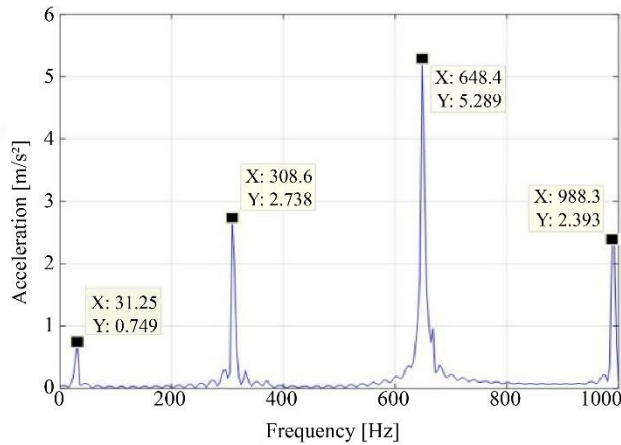


Fig. 9 Spectrum of gear vibration response with 50 μm eccentricity

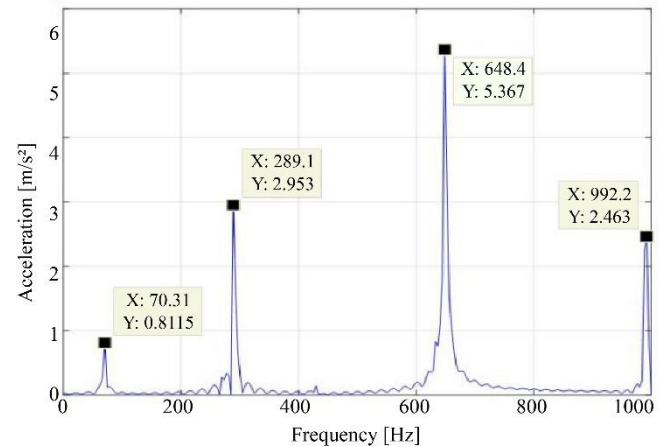


Fig. 11 Spectrum of gear vibration response with 100 μm eccentricity

However, the peaks observed in Figure 9 indicate the harmonics and characteristic frequencies of the system. The central peak indicates a resonance phenomenon likely related to a mechanical component such as a gear, bearings and shaft. The observation of several shifted peaks characteristic of the harmonic excitation generated by the rotating element, especially at 31.25 Hz, as well as at 308.6 Hz, 645.4 Hz and 988.3 Hz, indicates the presence of mechanical resonances. These observations may indicate cyclic disturbances such as imbalance, tooth irregularities (eccentricity) and even misalignment between the shafts.

In Figure 10, the signal clearly shows cyclic behavior with an envelope-like amplitude modulation. This phenomenon indicates a superposition of similar frequencies, resulting in a whipping effect characteristic of cyclic defects such as dynamic eccentricity, misalignment, and gear mesh. This indicates a system subjected to a high and continuous dynamic load. The vibration excitation maintains its intensity throughout the period, indicating a permanent rotational imbalance and continuous harmonic excitation, possibly related to coupling and transmission.

In Figure 11, the frequency spectrum analysis reveals several adverse acceleration peaks, characteristic of twitching responses preceded by a significant mechanical abnormality. The central peak appears at 648.4 Hz and has an estimated amplitude of 5.36 m/s^2 , indicating a dominant excitation frequency, which may result from an increased frequency resonance due to the eccentricity.

The second harmonic was observed at 289.1 Hz (2.95 m/s^2) and 992.2 Hz (2.46 m/s^2), indicating modulation of the capture signal caused by the repeated cycle of eccentricity effects. The presence of multiple harmonics, coupled with the relatively large amplitude of the peaks, confirms that a 100 μm eccentricity defect causes significant mechanical limitations. This defect causes a cyclic oscillation of the load transmitted between the teeth, creating quantified periodic oscillations over a wide frequency range.

Therefore, the time signal and frequency spectrum correlation shows that the system is experiencing significant mechanical vibrations, probably due to harmonic excitation associated with the rotating components. Such a vibration pattern should be analysed using time-frequency methods

(STFT, 3D Waterfall FFT, and RPM-frequency mapping) to localise the anomaly more accurately.

5.2. Fault Diagnosis in Gear Systems Using STFT, RPM-Frequency Mapping and 3D Waterfall FFT

For diagnostic accuracy, advanced signal processing techniques are necessary. The results of the simulated and gear responses were analyzed using STFT and RPM-frequency mapping and 3D Waterfall FFT.

Figure 12 shows a spectrogram of the vibration signal generated following a perfect gear tooth engagement. However, Figure 13 illustrates a 3D waterfall diagram highlighting the frequency spectrum of the gear vibration response, demonstrating that the machine is operating correctly.

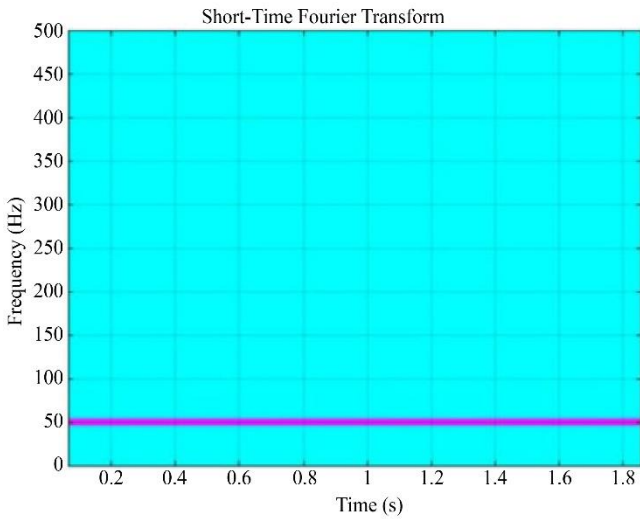


Fig. 12 STFT-vibration response of healthy gears

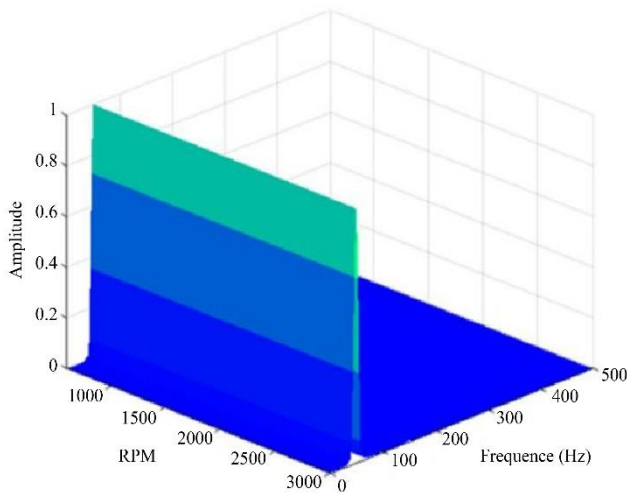


Fig. 13 A 3D frequency spectrum of healthy gears

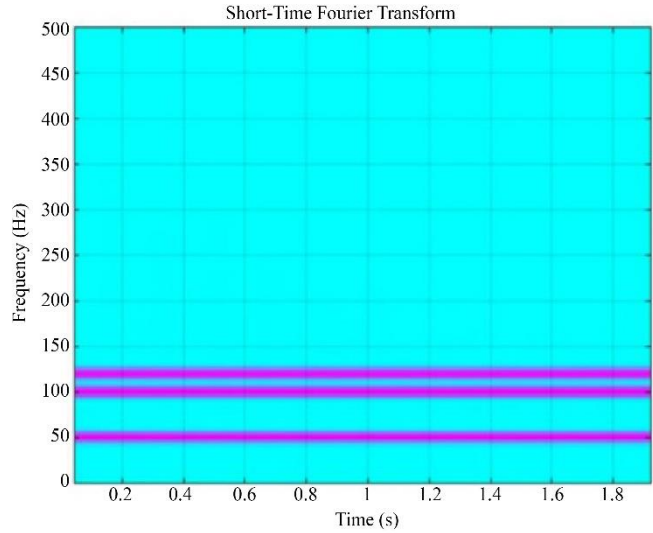


Fig. 14 STFT- gear vibration response at 50 μm eccentricity

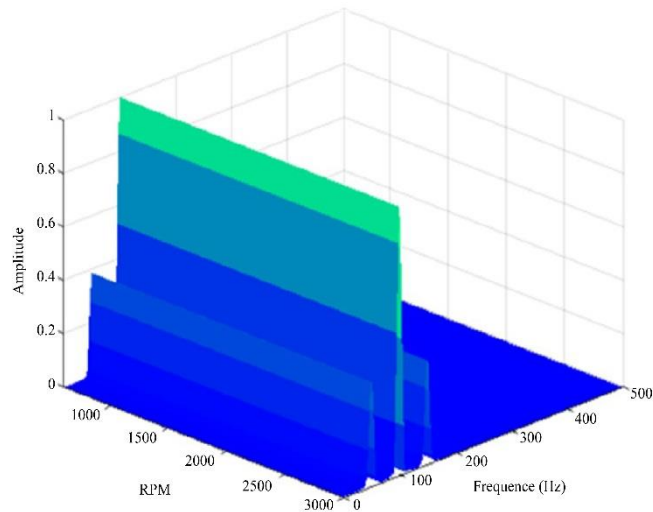


Fig. 15 3D frequency spectrum of gear with 50 μm eccentricity

In Figure 14, the spectrogram obtained by applying STFT to the vibration signal of the defective gear highlights the variations in the energy frequency bands produced by an eccentricity coefficient of 50 μm during the meshing of the regularly spaced gear teeth between 0 and 497 Hz. Figure 15 shows the first signs of failure associated with the 50 m eccentricity and the development of this defect, with many nonlinear reactions perceptible on the three-dimensional frequency spectrum. Figure 16 shows a shift of three energy frequency bands: band 1 shifted from 55 to 49 Hz, bands 2 and 3, 497 Hz from 148 to 150 Hz, and 300 to 325 Hz, demonstrating the variation of the eccentricity value to 100 μm . Figure 17 shows that significant amplitudes of the gear frequency are detected in the range of 0–500 Hz. A change in the activation of narrowband processes is also noticed due to the increase in eccentricity up to 100 μm .

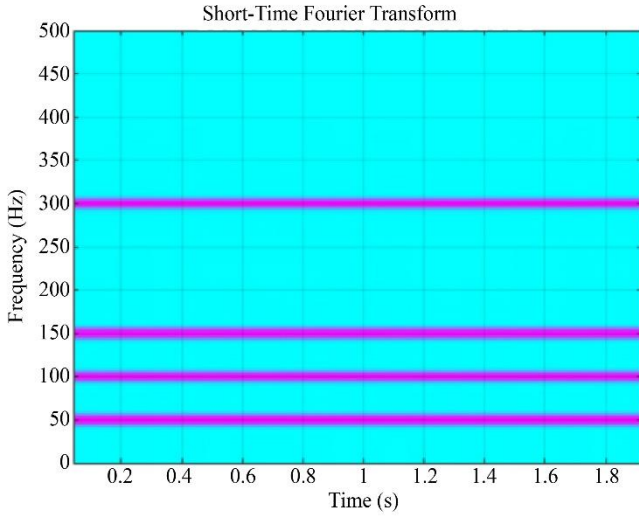


Fig. 16 STFT-vibration response of gear at 100 μm eccentricity

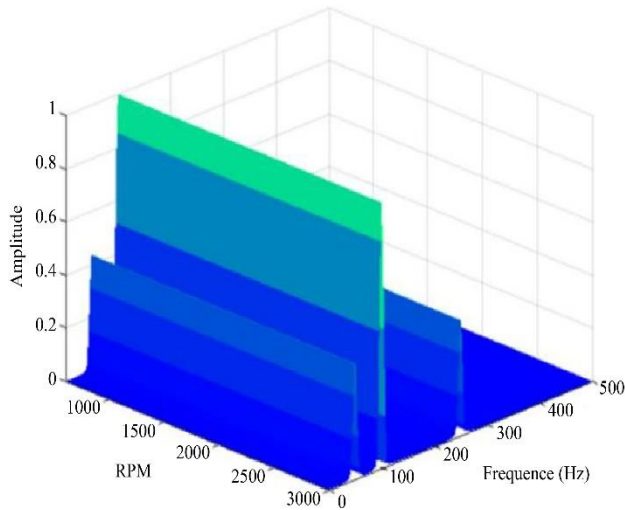
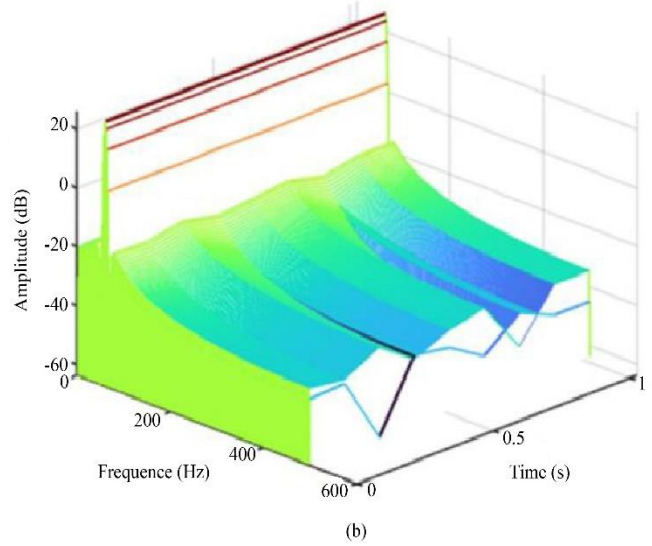


Fig. 17 3D frequency spectrum of gear with 100 μm eccentricity

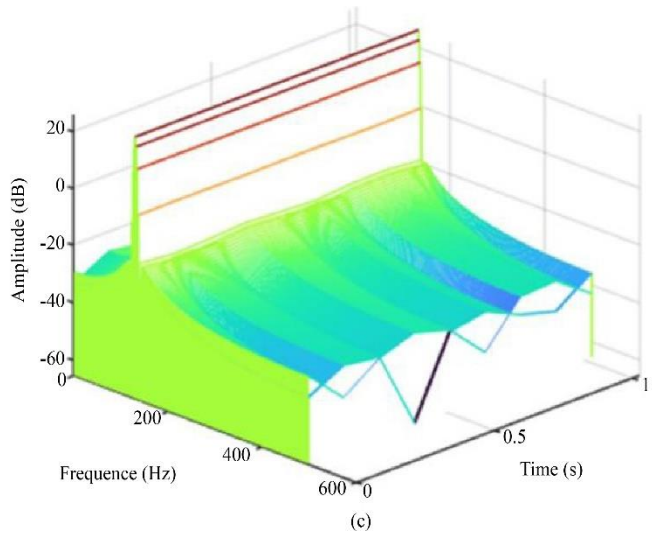
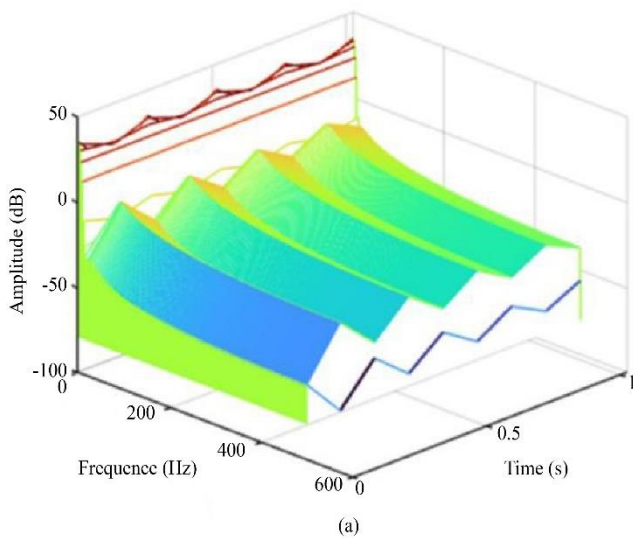


Fig. 18 3D waterfall FFT of lateral vibration response: (a) Healthy gear system, (b) Faulty gear system with 50 m eccentricity, and (c) 100 m eccentricity.



In Figure 18 (a), the spectrum remains stable throughout the analysed period. It is observed that soft and uniform bands form over time. These bands reflect constant mechanical harmonics, characteristic of the system's regular operation. A significant reduction in amplitudes is observed, reaching -100 dB above 400 Hz. The absence of clear peaks, distortions and random variations indicates no dynamic defect such as misalignment and eccentricity. In Figure 18 (b), it is observed that the overall structure remains relatively well-regulated, but some aspects indicate the presence of a minor problem compared to a perfect system.

The leading bands are still distinct, but they show intensity anomalies. Some frequencies are particularly noticeable, especially those between 200 and 400 Hz. This behaviour is typical of a moderate eccentricity defect of 50

micrometres. The defect creates cyclic forces that amplify the signal frequencies, which are related to the rotation speed of the gear system. It also notices that the high frequencies retain some energy but usually decrease rapidly in an intact system. This indicates that the energy in these regions is higher than expected, which could signal the beginning of slight degradation.

However, the spectrum tends to remain generally constant over time. In other words, the problem does exist, but it does not yet appear to be serious. In Figure 18 (c), a greater distortion of the frequency landscape is observed compared to a healthy and slightly defective system. The amplitude bands show less uniformity and increased irregularity, signalling enhanced vibration excitation in the system. Considerable amplification is observed in the frequency range between 100 Hz and 400 Hz, indicating that the more pronounced eccentricity defect produces stronger dynamic forces up to 100 micrometers. In addition, high-frequency energy is also present in notable quantities, characterized by a much slower amplitude damping, even beyond 500 Hz. This indicates that the system is undergoing significant degradation, likely impacting its optimal operation in the medium term.

5.3. Mesh Stiffness Evaluation for Gears without and with Eccentricity Faults

This study analysed the time-varying mesh stiffness of a two-stage spur gear system in healthy and different eccentricity faulty gear cases. For simplicity, the eccentricity is introduced in the first stage of the spur gear system. The diagram, as shown in Figure 19, illustrates the progression of gear stiffness as a function of the gear system's angular motion.

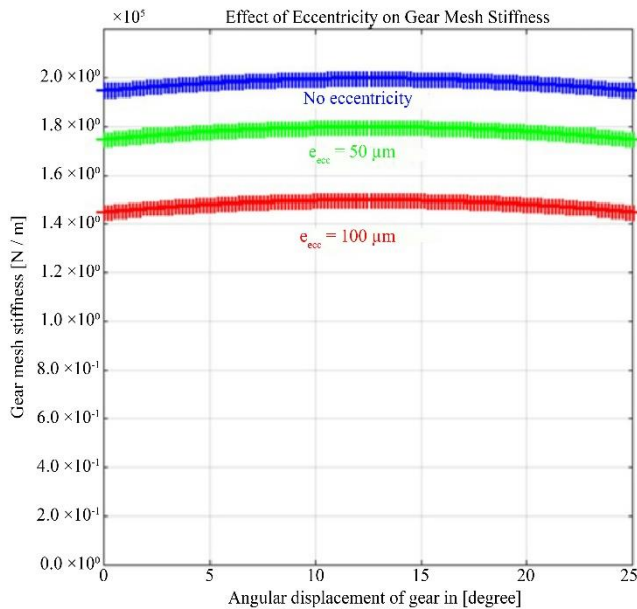


Fig. 19 Gear mesh stiffness with an eccentricity at different levels.

Figure 19 shows that the gear stiffness reduces significantly with increasing eccentricity. The gear stiffness approaches 2.0×10^5 N/m without eccentricity, indicating ideal tooth contact. At an eccentricity of $50 \mu\text{m}$, a significant decrease is observed; the stiffness decreases to about 1.75×10^5 N/m, and at an eccentricity of $100 \mu\text{m}$, the stiffness decreases continuously to about 1.5×10^5 N/m. This work shows that eccentricity negatively affects the mechanical stiffness of the gear contact, probably due to backlash fluctuations and temporary angular misalignments of the gear profiles.

6. Discussion

In the study, Yu et al. proposed a dynamically designed model based on a single rotor, which was designed considering local resources and profile imperfections. It is mainly based on finite element models combined with traditional frequency analysis, thus allowing for an efficient representation of structural defects on a large scale. However, this method is limited to identifying microdamages and rapidly fluctuating dynamics.

Contrary to the method used by Yu et al., the proposed approach consists of using STFT focused on the modulated frequency bands, even with an eccentricity of $50 \mu\text{m}$, as shown in Figure 14. This illustration shows a clear evolution of the frequency bands between 0 and 497 Hz in the grid phase, demonstrating the response of the STFT to standard values in a narrow range.

The ability of STFT to provide feature resolution allows one to understand local frequency changes associated with indirect dynamic progression, which is impossible with the global techniques used by Yu et al. without compromising accuracy. Wang et al. used the Finite Element Method (FEM) in conjunction with traditional Fast Fourier Transform (FFT) analysis to investigate dynamic transmission errors due to eccentricity. Their method provides a stable and complete result of the system frequency behavior, but cannot track fluctuations during transient phases and under variable loads.

As shown in Figures 15, 17 and 18, the RPM frequency, combined with 3D FFT waterfall analysis, is used not only to visualize the dominant frequency peaks associated with system anomalies, such as 645 Hz at $50 \mu\text{m}$ and 648 Hz at $100 \mu\text{m}$. These methods are crucial since they allow monitoring variations in harmonic characteristics to motor speed. The frequency and speed are shown in Figures 15 and 17. The results show the mutation and expansion of the frequency bands, clearly showing the temporal evolution of the fault. Figure 18, which shows a 3D FFT waterfall, shows an increase in distortion in the frequency bands from 100 Hz to 400 Hz as the eccentricity increases, a dynamic behavior that traditional FFT analysis cannot detect.

7. Conclusion

This study aims to investigate a nine-degree-of-freedom dynamic model for a two-stage drive system, with special attention to eccentricity anomalies. Accurate modelling based on the Lagrangian formula allows us to evaluate the effects of eccentricity on the stiffness and vibration response of the system. The vibration analysis and Time-frequency approach, such as the RPM-frequency map, 3D FFT waterfall and STFT, were used for efficient fault diagnostics in the spur gear system under various operational conditions.

The combination of RPM-frequency map, 3D FFT waterfall and STFT provide very effective in detecting short-term disturbances, including minor amplitude anomalies (50 μm). This method, which differs from classical frequency analysis methods, allows the detection of anomalies at a specific moment and tracking their development over time and according to the operating mode. The data show that the increase in eccentricity error (100 μm) leads to a significant decrease in coupling stiffness, an increase in oscillation harmonics, and a gradual deterioration of the spectrum, which

is observed in the frequency ranges from 100 to 500 Hz as shown in Figures 17 and 18. The dynamic evolution of vibration signals, which are difficult to detect with traditional methods (FFT), highlights the importance of time-frequency tools in the early diagnosis of mechanical defects. Finally, this study deepens our understanding of the nonlinear behavior caused by eccentricity errors in gear systems. It highlights the importance of using sophisticated analytical methods for more accurate condition diagnosis, which is the basis for industrial applications (power generation, aerospace and robotics) of predictive maintenance and intelligent monitoring of mechanical systems. Based on the results obtained, future research and practical applications can be conducted to enhance the field of diagnostics.

Acknowledgments

The authors are grateful for the resources and equipment provided by the Department of Industrial Engineering, Operation Management, and Mechanical Engineering at Vaal University of Technology (South Africa) to enable this work.

References

- [1] Olivier Petrilli et al., "Neural Network-Based Fault Detection Using Different Signal Processing Techniques as Pre-Process," *American Society of Mechanical Engineers (ASME), Structural Dynamics and Vibration*, vol. 70, pp. 97-101, 1995. [[Google Scholar](#)] [[Publisher Link](#)]
- [2] X. Gu, and P. Velex, "On the Dynamic Simulation of Eccentricity Errors in Planetary Gears," *Mechanism and Machine Theory*, vol. 61, pp. 14-29, 2013. [[CrossRef](#)] [[Google Scholar](#)] [[Publisher Link](#)]
- [3] P. Velex, and M. Maatar, "A Mathematical Model for Analysing the Influence of Shape Deviations and Mounting Errors on Gear Dynamic Behaviour," *Journal of Sound and Vibration*, vol. 191, no. 5, pp. 629-660, 1996. [[CrossRef](#)] [[Google Scholar](#)] [[Publisher Link](#)]
- [4] Wang Guangjian et al., "Research on the Dynamic Transmission Error of A Spur Gear Pair with Eccentricities by Finite Element Method," *Mechanism and Machine Theory*, vol. 109, pp. 1-13, 2017. [[CrossRef](#)] [[Google Scholar](#)] [[Publisher Link](#)]
- [5] A. Parey, and N. Tandon, "Spur Gear Dynamic Models Including Defects: A Review," *The Shock and Vibration Digest*, vol. 35, no. 6, pp. 465-478, 2003. [[Google Scholar](#)] [[Publisher Link](#)]
- [6] Emmanuel Rigaud, and Jean Sabot, "Effect of Elasticity of Shafts, Bearings, Casing and Couplings on the Critical Rotational Speeds of a Gearbox," *Proceedings of the International Conference of Gears*, Dresde, Germany, pp. 833-845, 1996. [[Google Scholar](#)] [[Publisher Link](#)]
- [7] Ankur Saxena, Anand Parey, and Manoj Chouksey, "Effect of Shaft Misalignment and Friction Force on Time-Varying Mesh Stiffness of Spur Gear Pair," *Engineering Failure Analysis*, vol. 49, pp. 79-91, 2015. [[CrossRef](#)] [[Google Scholar](#)] [[Publisher Link](#)]
- [8] Wennian Yu et al., "The Dynamic Coupling Behaviour of A Cylindrical Geared Rotor System Subjected to Gear Eccentricities," *Mechanism and Machine Theory*, vol. 107, pp. 105-122, 2017. [[CrossRef](#)] [[Google Scholar](#)] [[Publisher Link](#)]
- [9] Aijun Hu et al., "Dynamic Modeling and Analysis of Multistage Planetary Gear System Considering Tooth Crack Fault," *Engineering Failure Analysis*, vol. 137, 2022. [[CrossRef](#)] [[Google Scholar](#)] [[Publisher Link](#)]
- [10] Yifan Li et al., "Time-Frequency Ridge Estimation: An Effective Tool for Gear and Bearing Fault Diagnosis at Time-Varying Speeds," *Mechanical Systems and Signal Processing*, vol. 189, 2023. [[CrossRef](#)] [[Google Scholar](#)] [[Publisher Link](#)]
- [11] Hui Wang et al., "Intelligent Fault Diagnosis for Planetary Gearbox Using Time-Frequency Representation and Deep Reinforcement Learning," *IEEE/ASME Transactions on Mechatronics*, vol. 27, no. 2, pp. 985-998, 2022. [[CrossRef](#)] [[Google Scholar](#)] [[Publisher Link](#)]
- [12] Xinhao Tian, "Dynamic Simulation for System Response of Gearbox Including Localized Gear Faults," Theses and Dissertations, University of Alberta, 2004. [[Google Scholar](#)] [[Publisher Link](#)]
- [13] D.C.H. Yang, and J.Y. Lin, "Hertzian Damping, Tooth Friction and Bending Elasticity in Gear Impact Dynamics," *Journal of Mechanisms, Transmissions, and Automation in Design*, vol. 109, no. 2, pp. 189-196, 1987. [[CrossRef](#)] [[Google Scholar](#)] [[Publisher Link](#)]
- [14] P. Sainsot, P. Velex, and O. Duverger, "Contribution of Gear Body to Tooth Deflections-A New Bidimensional Analytical Formula," *Journal of Mechanical Design*, vol. 126, no. 4, pp. 748-752, 2004. [[CrossRef](#)] [[Google Scholar](#)] [[Publisher Link](#)]